Available online at www.sciencedirect.com
ScienceDirect
Journal of Physics and Chemistry of Solids 68 (2007) 1749–1755
JOURNAL OF PHYSICS AND CHEMISTRY OF SOLIDS
www.elsevier.com/locate/jpcs

Cr-doping effect on the structural, magnetic, transport properties and Raman spectroscopy of $La_{(2+x)/3}Sr_{(1-x)/3}Mn_{1-x}Cr_xO_3$ perovskites

W.J. Li[a], Bo Zhang[a,*], W. Lu[a], Y.P. Sun[b], Yuheng Zhang[b]

[a]National laboratory for Infrared Physics, Shanghai Institute of Technical Physics, Chinese Academy of Science, Shanghai 200083, PR China
[b]Key Laboratory of Materials Physics, Institute of Solid State Physics, Chinese Academy of Sciences, Hefei 230031, PR China

Received 29 August 2006; received in revised form 15 April 2007; accepted 23 April 2007

Abstract

A series of the double-doping samples $La_{(2+x)/3}Sr_{(1-4x)/3}Mn_{1-x}Cr_xO_3$ ($0 \leqslant x \leqslant 0.25$) with the Mn^{3+}/Mn^{4+} ratio fixed at 2:1 have been fabricated. The structural, magnetic, transport properties and Raman spectroscopy have been investigated, and no apparent crystal structure change is introduced by Cr doping up to $x = 0.25$. But the Curie temperature T_C and metal–insulator transition temperature T_{MI} are strongly affected by Cr substitution. The room temperature Raman spectra start exhibiting some new features following the increasing concentration of Cr substitutions. Moreover, it is worth noting that the frequency of the A_{1g} phonon mode can also be well correlated with the A-site mismatch effect (σ^2), which is influenced mainly by the variety of the Sr content.

PACS: 78.30.Hv; 71.30.+h; 75.47.Gk

Keywords: C. Raman spectroscopy

1. Introduction

Mixed-valence manganites with the perovskite structure have been studied for a long time. Early research was motivated by a need to develop insulating ferromagnets with a large magnetization for high-frequency applications. Recent renewed interest has focused on the negative colossal magnetoresistance (CMR) [1–3]. The basic structure, magnetic, and transport properties of $R_{1-x}A_xMnO_3$ (R = rare earth, A = Ca, Sr, Ba) were widely studied in the past years. Early works had revealed the importance of the double-exchange (DE) interaction [4] through Mn^{3+}–O–Mn^{4+} network as well as the strong electron–phonon coupling due to Jahn–Teller effect associated with Mn^{3+} ion in the CMR effect [5]. Besides, it is now clear that lattice strain and deformations, which affect the Mn^{3+}–O–Mn^{4+} bond angle and length, have dramatic consequences for the properties of these systems [6]. In terms of the crucial role of Mn site, it would be interesting and worthwhile to study the effects on Mn-site element substation, which can directly modify the Mn^{3+}–O–Mn^{4+} network and in turn largely affects their physical properties as well as CMR. There have been already considerable reports on the effects of Mn-site substitution by foreign elements such as Ni [7], Al [8], Ga [9], Cr [10], etc. Among these doping elements, Cr has a spectacular effect and attracts more attention. For instance, the doping on Mn site with 5% of Cr in the charge ordered (CO) insulator $Pr_{0.5}Ca_{0.5}MnO_3$ can destroy the CO antiferromagnetic (AFM) state and induces an insulator–metal (I–M) transition [11]. Recently, Sun et al. [12] performed a systematic study on the magnetic, electrical transport, and magnetoresistance properties of $La_{2/3}Sr_{1/3}Mn_{1-x}Cr_xO_3$ compounds. Some interesting results have also been presented. Although experiments have been successfully employed to investigate in the $La_{2-x}Sr_xCuO_4$ system [13], there are few results concerning Mn-substitution having the fixed ratio of Mn^{3+}/Mn^{4+} on $La_{(2+x)/3}Sr_{(1-x)/3}Mn_{1-x}Cr_xO_3$ system. In order to explore further the doping

*Corresponding author. Tel.: +86 21 6542 0850x24105; fax: +86 21 6583 0734.
E-mail addresses: jwli@issp.ac.cn (W.J. Li), bozhang@mail.sitp.ac.cn (B. Zhang).

0022-3697/$ - see front matter © 2007 Elsevier Ltd. All rights reserved.
doi:10.1016/j.jpcs.2007.04.021

effect of Cr, vibration modes of $Mn(Cr)O_6$ octahedrons have also been investigated by means of Raman spectra measurements because the vibration modes are sensitive to the substitution. In this paper, a series of double-doping samples $La_{(2+x)/3}Sr_{(1-x)/3}Mn_{1-x}Cr_xO_3$ ($0 \leqslant x \leqslant 0.25$) have been successfully synthesized. The structural, magnetic, transport properties and Raman scattering measurements on $La_{(2+x)/3}Sr_{(1-x)/3}Mn_{1-x}Cr_xO_3$ polycrystalline samples have been systematically investigated.

2. Experiments

As we know, in $R_{1-x}A_xMnO_3$ compounds, there is an I–M transition associated with a paramagnetic–ferromagnetic (PM–FM) transition for $0.2 < x < 0.5$. But, it has been generally recognized that the $Mn^{3+}/Mn^{4+} = 2{:}1$ was the optimum ratio. Therefore, we fabricated the polycrystalline $La_{(2+x)/3}Sr_{(1-x)/3}Mn_{1-x}Cr_xO_3$ samples, which are called double-doped samples, so that, regardless of the matter x varieties, the $Mn^{3+}/Mn^{4+} = 2{:}1$ was maintained. Due to the different of ionic radii for the La, Sr, Mn^{3+}, Mn^{4+} and Cr, the tolerance factor t will change with x change. As shown in Table 2. With increasing of x, t increase for single doping and t decrease for double doping.

Polycrystalline $La_{(2+x)/3}Sr_{(1-x)/3}Mn_{1-x}Cr_xO_3$ ($0 \leqslant x \leqslant 0.25$) samples, were prepared through the conventional solid-state reaction method in air. Appropriate proportions of high purity La_2O_3, $SrCO_3$, MnO_2, and Cr_2O_3 powders were thoroughly mixed according to the desired stoichiometry, and then prefired at 900 °C for 24 h. Afterwards the powder was ground and heated at 1250 °C for 24 h, then, the powders obtained were ground, pelletized, and sintered at 1350 °C for another 24 h with three intermediate grinding, and finally, the furnace was cooled down to room temperature.

The crystal structures were examined by X-ray diffractometer using Cu Kα radiation at room temperature. The magnetic measurement was carried out with a quantum design superconducting quantum interference device (SQUID) MPMS system ($2\,K \leqslant T \leqslant 400\,K$, $0 \leqslant H \leqslant 5\,T$). The resistance as a function of temperature (under zero) was measured by the standard four-probe method in a commercial physical property measurement system (Quantum Design PPMS) from 5 to 400 K.

The crystal structures and phase purity were examined by X-ray diffractometer using Cu Kα radiation at room temperature. Unpolarized Raman experiments at room temperature were carried out in the back scattering geometry by using a Dilor LabRam-Infinity micro-Raman system equipped with a cooled coupled charged device (CCD) for light detection. The samples were excited with the 632.8 nm laser line from a He–Ne laser. The elastic scattering was rejected with a Notch filter, and the Raman signal was analyzed by the grating of the spectrometer. The laser power in the focus spot being kept below 1 mW/cm^2 to avoid overheating of the samples.

3. Results and discussion

The powder X-ray diffraction at room temperature shows that all samples under investigation are single phase without detectable secondary phases and the samples have a rhombohedral lattice with the space group $R\bar{3}C$. The structural parameters of the samples are refined by the standard Rietveld technique [14]. The obtained structural parameters are listed in Table 1. Fig. 1(a) and (b) show the experimental and calculated XRD patterns for $x = 0.10$ and 0.25 samples, respectively. No structural transition has been observed and the lattice parameters for $La_{(2+x)/3}Sr_{(1-x)/3}Mn_{1-x}Cr_xO_3$ ($0 \leqslant x \leqslant 0.25$) samples vary nearly monotonically with increasing Cr content. The Mn–O–Mn bond angle decreases with increasing Cr-doping level, whereas the Mn–O bond length increase displays the inverse correlation to the variation in the Mn–O–Mn bond angle. Taking into account the substitution defects in the B cationic sublattice introduce different types of disorder, and the departure from the average Mn radius R (Mn_{av}) (defined as the average over the radii for Mn^{3+} and Mn^{4+} ions in the ratio $(1-x)$: x in $R_{1-x}A_xMnO_3$ compounds) at the dopant site would subject the neighboring Mn–O bonds to a centric push or pull [11]. When a bigger ion at the Mn site should compress the neighboring Mn–O bonds and result in decreasing the Mn–O–Mn bond angle. Therefore, based on the monotonic varying of Mn–O bond length, lattice volume and Mn–O–Mn bond angle with increasing Cu-doping level, it is reasonable to consider that Cr ions are as Cr^{3+}, for R (Cr^{3+}) > R (Mn_{av}), R (Sr^{2+}) < R (La^{3+}).

Fig. 2 presents the temperature dependence of magnetization M for $La_{(2+x)/3}Sr_{(1-x)/3}Mn_{1-x}Cr_xO_3$ ($0 \leqslant x \leqslant 0.2$) under zero-field cooling (ZFC) modes. All samples display a PM to FM phase transition. Meanwhile, the range of the

Table 1
Refined structural parameters of $La_{(2+x)/3}Sr_{(1-x)/3}Mn_{1-x}Cr_xO_3$ ($0 \leqslant x \leqslant 0.25$) samples at room temperature

Parameters	$x = 0.00$	$x = 0.05$	$x = 0.10$	$x = 0.15$	$x = 0.20$	$x = 0.25$
a (Å)	5.4677	5.4689	5.4707	5.4834	5.5054	5.5293
c (Å)	13.4856	13.4967	13.5021	13.5318	13.6526	13.7162
Mn–O (Å)	1.9467	1.9501	1.9580	1.9633	1.9747	1.9990
Mn–O–Mn (°)	168.88	167.44	166.31	163.94	159.67	158.19
V (Å^3)	349.152	349.593	349.967	352.362	358.253	363.170

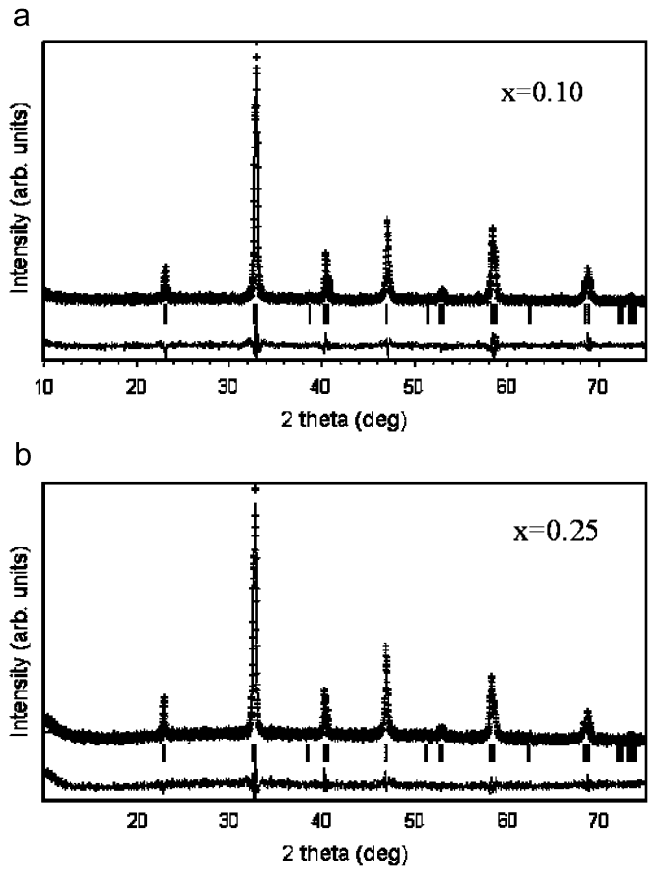

Fig. 1. X-ray diffraction pattern of $La_{(2+x)/3}Sr_{(1-x)/3}Mn_{1-x}Cr_xO_3$ samples: (a) $x = 0.10$; (b) $x = 0.25$ are shown. Crosses indicate the experimental data and the calculated profile is the continuous line overlying them. The lowest curve shows the difference between experimental and calculated patterns. The vertical bars indicate the expected reflection positions.

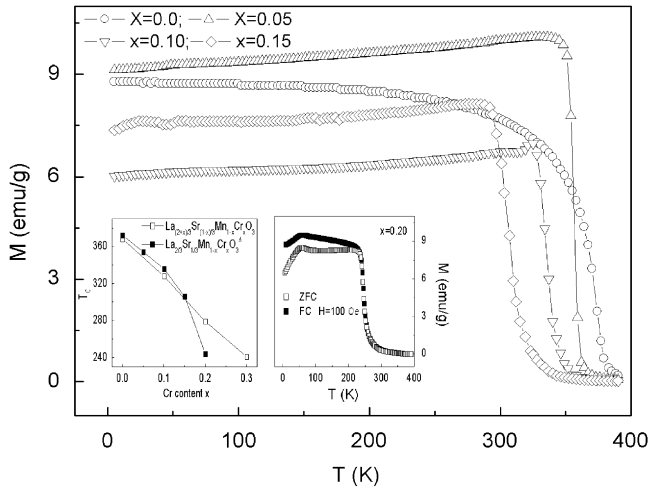

Fig. 2. The temperature dependence of magnetization is $La_{(2+x)/3}Sr_{(1-x)/3}Mn_{1-x}Cr_xO_3$ ($0 \leqslant x \leqslant 0.2$) measured in a zero field is shown. The inset is the variation of T_C with x. The data of $La_{2/3}Sr_{1/3}Mn_{1-x}Cr_xO_3$ series (denoted by the Δ) are quoted from Ref. [12].

magnetic transition is broadened with increasing Cr contents. The Curie temperature T_C, which is defined as the one corresponding to the peak of dM/dT vs T curve, decreases more rapidly with increasing Cr content than that reported corresponding single-doping samples of $La_{2/3}Sr_{1/3}Mn_{1-x}Cr_xO_3$ (See the inset of Fig. 2.), especially for the heave doping samples, where, T_C decreases slowly with increasing Cr content, so that T_C is still above 241 K for $x = 0.3$ sample.

The difference in magnetic transition temperature between the single-doping and double-doping samples is because, for the double-doping samples, with the doping level increasing, the Sr content also gradually decreases, as a result, the tolerance factor t decreases more rapidly (see Table 2), and t is defined as $(\langle r_A\rangle + \langle r_O\rangle)/\sqrt{2}(\langle r_B\rangle + \langle r_O\rangle)$ [5], where $\langle r_A\rangle$ is the average ionic radius of A-site ions (La^{3+} and Sr^{2+}) and $\langle r_B\rangle$ is the average ionic radius of the B-site ions (Mn and Cr). The tolerance factor is $t = 1$ for spherical ions packed in the ideal perovskite structure (Mn–O–Mn angle would be 180°). Moreover, t becomes smaller for the samples $La_{(2+x)/3}Sr_{(1-x)/3}Mn_{1-x}Cr_xO_3$ and the lattice becomes more distorted with doping increasing, this means that the Mn–O–Mn angle deviates from 180°, which leads to a reduction of the DE interaction. It is contrary for the samples $La_{2/3}Sr_{1/3}Mn_{1-x}Cr_xO_3$, the t increases with doping increasing, to a certain extent, which will be in favor of the DE interaction. Obviously, for our studied systems, the influence of t on magnetic properties plays a dominant role, which leads to the rapid decrease of T_C. (See the inset of Fig. 2.) It notes that the maximum of magnetization in a zero-field cool keeps increasing from $x = 0$ to 0.05, then it goes down with further Cr content. The similar results have been reported for the Cr doped compound [15], which may be the reason that our samples are polycrystalline, some extrinsic factors such as grain size and boundary cannot be excluded to be responsible for it. In order to clarify the AFM component may develop at low temperature for highly doped sample $x = 0.2$, field-cooled (FC) $M(T)$ was also measured and illustrated the inset of Fig. 2. It is clear that the ZFC magnetization data do not coincide with FC data below TC, which is a characteristic of cluster glass [16].

For $La_{2/3}Sr_{1/3}MnO_3$ sample, it shows metallic behavior below 380 K as reported before [17]. When Mn is partly substituted by Cr, the system displays a complicated and interesting transport behavior. Fig. 3 demonstrates the temperature dependence of resistivity for the double-doping samples with $x = 0$, 0.05, 0.10, 0.15, and 0.20 at zero field in the temperature of 5–400 K. Comparing with the reported single-doping samples, for the double-doping samples, one can see that there are obviously different transport behaviors, especially, one can see that when x reaches 0.15, the I–M transition still exhibits in ρ–T curve and the transition temperature T_{P1} is near 309 K for the double-doping sample. However, for the same content single-doping sample, no insulating-metallic transition occurs. A minimum in the $\rho(T)$ curves is also observed

Table 2
The tolerance factor t, A-site average ionic radius $\langle r_A \rangle$, and A-site mismatch factor δ^2 as a function of x

Parameters	$x = 0.00$	$x = 0.05$	$x = 0.10$	$x = 0.15$	$x = 0.20$	$x = 0.25$
Single doping t (Å)	1.253	1.252	1.250	1.248	1.247	1.245
Double doping t (Å)	0.93495	0.93419	0.93342	0.93264	0.93188	0.93110
$\langle r_A \rangle$	1.253	1.252	1.250	1.248	1.247	1.245
δ^2	0.00222	0.002164	0.0021	0.002039	0.001947	0.001875

According to the Shannon radii: $r_{Cr^{3+}} = 0.615$ Å, $r_{Mn^{3+}} = 0.645$ Å, $r_{Mn^{4+}} = 0.530$ Å, $r_{La^{3+}} = 1.22$ Å, $r_{Sr^{2+}} = 1.32$ Å.

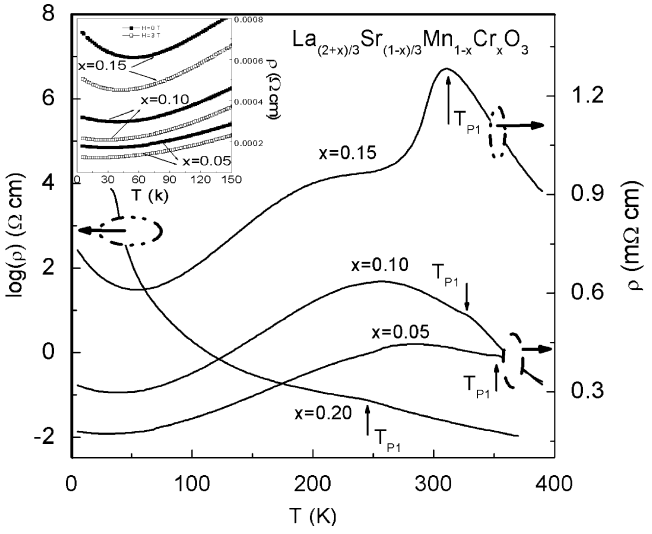

Fig. 3. The resistivity versus temperature curves of $La_{(2+x)/3}Sr_{(1-x)/3}Mn_{1-x}Cr_xO_3$ ($0 \leqslant x \leqslant 0.2$) samples. The inset is the magnifying plot of low-temperature resistivity.

for the measurement made at zero fields. This result is similar to that obtained on doped ceramic manganites such as $La_{0.5}Pb_{0.5}MnO_3$ [18]. Two typical models are considered to account for this minimum: (i) bulk scattering with quantum corrections to conductivity [19,20] and (ii) intergrain tunneling [18]. In the first model, it predicts a weak dependence of the low-T resistivity on magnetic field in the range of interest, which is dissatisfied with the following experiments, where the low-temperature resistivity is highly sensitive to the external field. As can be seen from the inset of Fig. 3, under zero magnetic field, $T_{min} \approx 34$, 38, and 54 K, but under 3 T magnetic field, $T_{min} \approx 21$, 27, and 43 K, for $x = 0.05$, 0.10, and 0.15, respectively. In the second model, the nature of the resistivity upturn at low temperature is attributed to the increased AFM correlation between grains [18]. The application of magnetic fields mainly causes the rotation of the 'partial' grain moments to a unique direction along the magnetic field, resulting in a suppression of the resistivity upturn, and hence the resistivity minimum shifts to lower temperature and the magnitude of the resistivity decreases.

The different transport behaviors are interesting but have not been well understood, yet. It is generally considered that a stronger DE always corresponds to a higher transition temperature T_{p1}. To date, the following three factors have been shown to strongly affect the T_{p1} [21], i.e., the hole carriers density controlled by the Mn^{3+}/Mn^{4+} ratio, the A-site cation size $\langle r_A \rangle$, and the A-site mismatch effect (σ^2) defined by $\sigma^2 = \sum y_i r_i^2 - \langle r_A \rangle^2$. In contrasted with the polycrystalline samples of $La_{2/3}Sr_{1/3}Mn_{1-x}Cr_xO_3$, for the $La_{(2+x)/3}Sr_{(1-x)/3}Mn_{1-x}Cr_xO_3$ ($0 \leqslant x \leqslant 0.25$) samples, the stoichiometrical compositions for all metallic ions are varied with the Cr doping, as a result, variations in $\langle r_A \rangle$ and σ^2 (shown in Table 1). It can be seen that both $\langle r_A \rangle$ and σ^2 decrease with increasing the Cr doping content. Decreasing $\langle r_A \rangle$ would weaken the DE mainly due to the decreasing of the one-electron e_g band, while the decrease of σ^2 would prevent the localization of e_g electrons thereby strengthen the DE. The competition between $\langle r_A \rangle$ and σ^2 can be well reflected the variation of T_{p1} with Cr doping content. In other words, the influence induced by $\langle r_A \rangle$ and σ^2 may be main factor for the variation of T_{p1}. It is also the reason that the metallic-insulating transition still occurs for $x = 0.15$ sample. We also note that, similar to the reported Cr doping samples $La_{0.67}Ca_{0.33}Mn_{1-x}Cr_xO_3$ [15] and $Pr_{0.5}Ca_{0.5}Mn_{1-x}Cr_xO_3$ ($y = 0.10$) [22], the double-bumps feature of $\rho(T)$ curve was also observed in double-doping samples $La_{(2+x)/3}Sr_{(1-x)/3}Mn_{1-x}Cr_xO_3$. From these consistent results we can conclude that this double-bumps feature of resistivity is intrinsic and originates from the crucial role of Cr element. The peak that lies very near T_C originates from the same mechanism based on the DE between Mn ions as in undoped $La_{2/3}Sr_{1/3}MnO_3$. The second peak grows with increasing Cr content. Therefore, it should be ascribed to the crucial role of Cr. Due to the identical electronic configuration between Cr^{3+} and Mn^{4+}, there is a possibility of the occurrence of DE through Mn^{3+}–O–Cr^{3+}. This view could be supported by the reported results of CMR behavior [17].

The room temperature Raman spectra of $La_{(2+x)/3}Sr_{(1-x)/3}Mn_{1-x}Cr_xO_3$ ($0 \leqslant x \leqslant 0.25$) samples with different Cr contents are shown in Fig. 4. The undoped sample (lower spectrum in Fig. 4) presents a rhombohedral crystal structure belonging to the space group $D_{3d}^6(R\bar{3}C)$. Thirty vibrational degrees of freedom at the Γ point are distributed among the

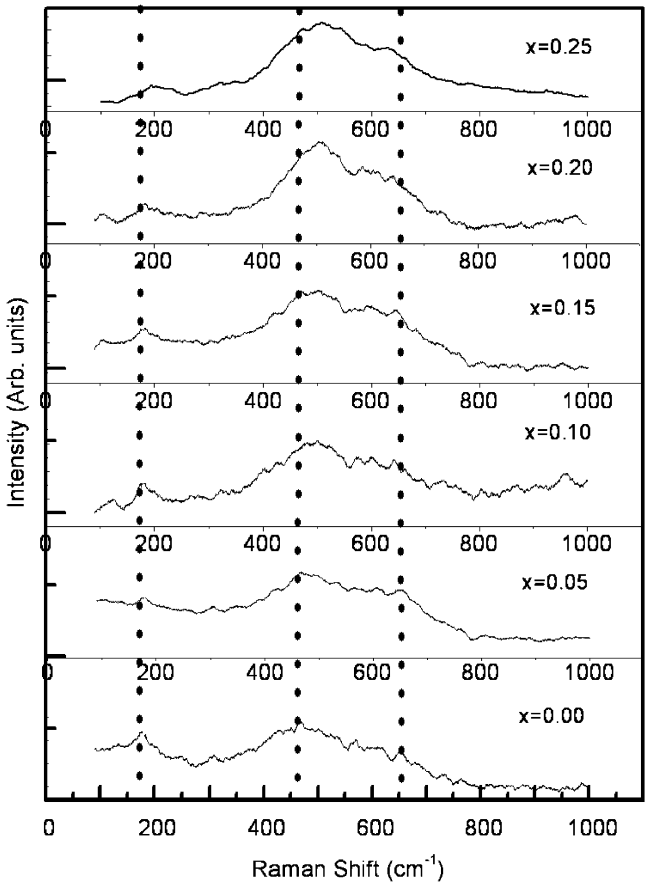

Fig. 4. Unpolarized Raman spectra taken at room temperature in different $La_{(2+x)/3}Sr_{(1-x)/3}Mn_{1-x}Cr_xO_3$ ($0 \leqslant x \leqslant 0.2$) samples. The labels and numbers stand for mode symmetry assignment and frequencies in units of cm^{-1}. Dotted lines denote the position of the three observed Raman-active modes at the room temperature for $x = 0$ sample.

irreducible representation as

$$\Gamma(D_{3d}^6) = 2A_{1u} + 3A_{2g} + A_{1g} + 4A_{2u} + 4E_g + 6E_u, \quad (1)$$

where only five ($A_{1g} + 4E_g$) modes are Raman active. For $x = 0$, the three observed Raman-active modes located at about 175, 464, and 653 cm^{-1} (marked with dotted lines). Polarized Raman scattering experiments performed on $La_{0.7}Sr_{0.3}MnO_3$ single crystals combined with lattice dynamics studies indicate that the mode at near 175 cm^{-1} is an A_{1g} symmetry mode. The isotope oxygen substitution shows that it is pure oxygen mode [23]. Moreover, many groups assign it as "soft" rotational for the octahedral mode that explains the large changes of its frequency changing the distortions of the perovskite [24–27]. The mode at near 464 cm^{-1} is obviously similar to the mode M4 in $La_{0.7}Ca_{0.3}MnO_3$ [28], both showing a E_g character. It has been correlated with the out-of-phase oxygen-bending mode near 480 cm^{-1} in $LaMnO_3$ [23].

Concerning the peaks at near 660 cm^{-1}, Podobedov et al. [29] suggests that the 660 cm^{-1} peak probably related to one of the simple oxides like that of lanthanum or manganese. Moreover, this mode is very broad in all manganites, which is evidence that they are full-band modes, rendered Raman active by disorder Jahn–Teller distortions [30,31].

In order to illustrate the change of the Raman spectra with doping content x in detail, the frequencies of the experimental peaks are plotted with doping level for E_g mode and A_{1g} mode in Fig. 5(a), (b), respectively. The spectra start exhibiting the following main features with increasing Cr content. First, the A_{1g} and symmetry E_g mode hardens, and the intensity of the E_g symmetry mode gradually increases. Second, a higher frequency mode emerges at near 653 cm^{-1} and shows a noticeable softening.

It is also evident that E_g mode is significantly broader than the rare-earth A_{1g} mode, assistant with the general belief that the disorder in these systems is primarily associated with the MnO_6 octahedra. Further increasing of the intensity of the mode at near 465 cm^{-1} is an indicative that the degree of disorder is increasing, since Cr atoms are replacing. It is reasonable that in our studied samples, with increasing Cr content, $\langle r_A \rangle$ gradually decreases. The decrease of the ionic radius $\langle r_A \rangle$ results in the lattice becomes more distorted. The strong local

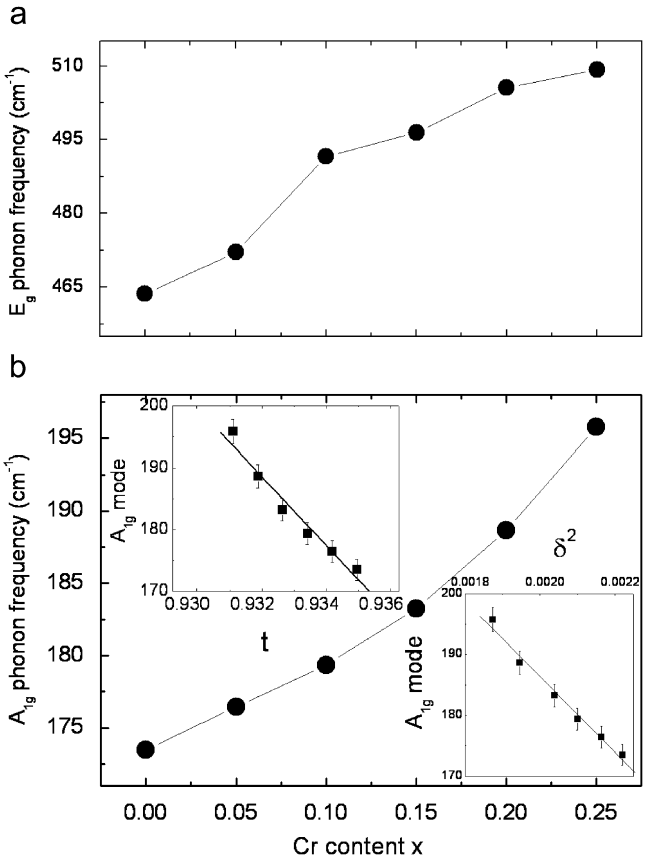

Fig. 5. The frequencies of the experimental peaks are plotted with doping level in the $La_{(2+x)/3}Sr_{(1-x)/3}Mn_{1-x}Cr_xO_3$ samples: (a) the E_g symmetry mode; (b) the A_{1g} mode. In the inset, the A_{1g} frequency shift is plotted as function of the toleration factor t and A-site mismatch factor δ^2, respectively.

stress produced by these defects can be alleviated through $Mn(Cr)O_6$ octahedral rotate in association with rotations of the neighboring octahedra, which strongly affects the force constant in the La/Sr–MnO_6 vibrational system. This effect explains the corresponding change in the Raman shift of the related E_g frequency mode.

At higher doping the observed A_{1g} mode Raman spectra (Fig. 5(b)) reveal a reduction of the scattering intensity, and an evident shift of the position of peak. From Fig. 5(b), it follows that this peak undergoes a strong (about $25\,cm^{-1}$) change in Raman shift as the doping content increase from 0 to 0.25. Amelitchev et al. [28] shows A_{1g} symmetry is related of the vibrations of A-site cations. However, for our studied double-doping samples, the simultaneous introduction of substitutional defect in the B-site and A-site has a strong effect in the structural change of the lattice due to different ionic radii. So, we consider that the observed frequency shift is determined by the distortions introduced by the A-site and B-site substitutions. The inset of Fig. 5(b) shows the dependence of the A_{1g} mode frequency on the tolerance factor t values. Within the errors, it can be concluded that the band shift is a linear function of the tolerance factor for our studied samples. A similar behavior is found [28]. Moreover, it is more worth noting that the frequency of the A_{1g} mode can also be well correlated with the A-site mismatch effect (σ^2), which is influenced mainly by the variety of the Sr content. The linear relationship of the frequency shift if the σ^2 is also shown in inset of Fig. 5(b). So, it can be concluded that the band shift is a linear function of t and σ^2.

4. Summary and conclusions

We have used X-ray diffractometer, magnetic, transport measurement, and Raman spectroscopy to study the influence of Mn-site substitutions on samples $La_{(2+x)/3}Sr_{(1-4x)/3}Mn_{1-x}Cr_xO_3$ ($0 \leqslant x \leqslant 0.25$) with the Mn^{3+}/Mn^{4+} ratio fixed at 2:1. The result of the Rietveld refinement of X-ray powder diffraction shows that these compounds crystallize in a rhombohedral structure with the space group $R\bar{3}C$, and no apparent crystal structure change is introduced by Cr doping up to $x = 0.25$. By comparing with the reported single-doping samples, it is evident that the Curie temperature T_C and metal–insulator transition temperature T_{MI} are more strongly affected by Cr substitution. The room temperature Raman data of Cr substituted $La_{(2+x)/3}Sr_{(1-x)/3}Mn_{1-x}Cr_xO_3$ ($0 \leqslant x \leqslant 0.25$) system has been presented. For $x = 0$, the three observed Raman-active modes located at about 175, 464, and $653\,cm^{-1}$, respectively. Moreover, these spectra start exhibiting some new features following with the increasing concentration of Cr. Our results suggest that all of these properties are mainly determined by the structural disorder introduced by the substitutional defect in the B-site and A-site. The strong local stress produced by these defects can be alleviated through $Mn(Cr)O_6$ octahedral rotate in association with rotations of the neighbouring octahedral, which results in different magnetic, transport properties and Raman spectra. Furthermore, we have found that, for our studied double doping samples, the frequency shift of the A_{1g} phonon mode also depends linearly on the A-site mismatch factor σ^2, which is influenced mainly by the variety of the Sr content.

Acknowledgments

The work was supported by the National Natural Science Foundation of China through Grant no. 10474107 is acknowledged.

References

[1] R. von Helmolt, J. Wecker, B. Holzapfel, L. Schultz, K. Samwer, Phys. Rev. Lett. 71 (1993) 2331.
[2] K. Chahara, T. Ohno, M. Kasai, Y. Kosono, Appl. Phys. Lett. 63 (1993) 1990.
[3] S. Jin, T.H. Teifel, M. McCormack, R.A. Fastnacht, R. Ramesh, L.H. Chen, Science 264 (1994) 413.
[4] C. Zener, Phys. Rev. 82 (1951) 403.
[5] J. Millis, P.B. Littlewood, B.L. Shraiman, Phys. Rev. Lett. 74 (1995) 5134.
[6] H.Y. Hwang, S.-W. Cheong, P.G. Radaeli, M. Marezio, B. Batlogg, Phys. Rev. Lett. 77 (1995) 914.
[7] J.-W. Feng, L.-P. Hwang, Appl. Phys. Lett. 75 (1999) 1592.
[8] J. Blasco, J. Garcia, J.M. De Teresa, M.R. Ibarra, J. Perez, P.A. Algarabel, C. Marquina, C. Ritter, Phys. Rev. B 55 (1997) 8905.
[9] Y. Sun, X.L. Xu, Y. Zhang, Phys. Rev. B 60 (1999) 12317.
[10] L. Pi, S. Hebert, C. Yaicle, C. Martin, A. Maignan, B. Raveau, J. Phys.: Condens. Matter 15 (2003) 2701.
[11] Maignan, F. Damay, A. Barnabe, C. Martin, M. Hervieu, B. Raveau. Philos. Trans. R. Soc. London A 356 (1998).
[12] Y. Sun, W. Tong, X. Xu, Y. Zhang, Appl. Phys. Lett. 78 (2001) 643.
[13] C. Zhang, Y. Zhang, Phys. Rev. B 68 (2003) 054512.
[14] D.B. Wiles, R.A. Young, J. Appl. Crystallogr. 14 (1981) 149.
[15] Y. Sun, X. Xu, Y. Zhang, Phys. Rev. B 63 (2000) 054404.
[16] J.A Mydosh, In: Spin Glass: An Experimental Introduction, Taylor & Francis, London, 1993.
[17] W.J. Li, B.Ch. Zhao, R. Ang, W.H. Song, Y.P. Sun, Y. Zhang, Solid State Commun. 135 (2005) 467.
[18] N. Zhang, W. Ding, W. Zhong, D. Xing, Y.-W. Du, Phys. Rev. B 56 (1997) 8138.
[19] E. Rozenberg, M. Auslender, I. Felner, G. Gorodetsky, J. Appl. Phys. 88 (2000) 2578.
[20] A. Barnab, M. Ghosh, S. Biswas, S.K. De, S. Chatterjee, J. Phys.: Condens. Matter 10 (1998) 9799.
[21] L.M. Rodriguez-Martinez, J. Paul. Attfield, Phys. Rev. B 54 (1996) 15622.
[22] B. Raveau, A. Maignan, C. Martin, J. Solid State Chem. 130 (1997) 162.
[23] J.C. Irwin, J. Chrzanowski, J.P. Franck, Phys. Rev. B 59 (1999) 9362.
[24] M.N. Iliev, M.V. Abrashev, H.G. Lee, V.N. Popov, Y.Y. Sun, C. Thomsen, R.L. Meng, C.W. Chu, Phys. Rev. B 57 (1998) 2872.
[25] E. Granado, N.O. Morena, A. Garcma, J.A. Sanjurjo, C. Rettori, I. Torriani, S.B. Oseroff, J.J. Neumeier, A.K.J. McClellan, S.W. Caheong, Y. Tokura, Phys. Rev. B 58 (1998) 11435.
[26] L. Martín-Carrón, A. de Andrés, M.J. Martínez-Lope, M.T. Casais, J.A. Alonzo, Phys. Rev. B 66 (2002) 174303.
[27] M.V. Abrashev, A.P. Litvinchuk, M.N. Iliev, R.L. Meng, V.N. Popov, V.G. Ivanov, R.A. Chakalov, C. Thomsen, Phys. Rev. B 59 (1999) 4146.

[28] V.A. Amelitchev, B. Güttler, O.Yu. Gorbenko, A.A. Bosak, A.Yu. Ganin, Phys. Rev. B 63 (2001) 104430.
[29] V.B. Podobedov, D.B. Romero, A. Weber, J.P. Rice, R. Schreekala, M. Rajeswari, R. Ramesh, T. Venkatesan, H.D. Drew, Appl. Phys. Lett. 73 (1998) 3217.
[30] A.E. Pantoja, H.J. Trodahl, R.G. Buckley, Y. Tomioka, Y. Tokura, J. Phys.: Condens. Matter 13 (2001) 3741.
[31] L. Martín-Carrón, A. de Andrés, Eur. Phys. J B 22 (2001) 11.